MIMO channels in suburban environments at 300 MHz - analysis and modeling

Zhu, Meifang; Tufvesson, Fredrik; Eriksson, Gunnar

2012

MIMO Channels in Suburban Environments at 300 MHz - Analysis and Modeling

Meifang Zhu, *Student Member, IEEE,* Gunnar Eriksson, *Member, IEEE,*
and Fredrik Tufvesson, *Senior Member, IEEE*

Abstract

The COST 2100 channel model is a geometry based stochastic channel model (GSMC) for multiple-input multiple-output (MIMO) simulations. This paper presents parameterization and validation of the COST 2100 channel model for peer-to-peer communication in the 300 MHz band. Measurements were carried out in semi-rural and suburban environments for both line-of-sight (LOS) and non line-of-sight (NLOS) scenarios. The COST 2100 channel model is characterized and parameterized based on clusters. The KpowerMeans algorithm and a Kalman filter were used for identifying and tracking clusters from measurements. General issues regarding the parameterization for the COST 2100 channel model are analyzed in detail. A full set of single-link parameters for the channel model is extracted from the measurements. These parameters are used as the input to the channel model validation processes, targeting delay spread, spatial correlation, singular value distribution as well as antenna correlation. The validation results show good agreements for spatial correlation and channel capacity between the COST 2100 channel model and the 300 MHz outdoor measurements. Our findings suggest that the model has potential for modeling 300 MHz channels in outdoor environments, although some adjustments are needed for the distribution of cluster delay spreads and the size of visibility regions.

Index Terms

Parameterization, validation, MIMO, outdoor, COST 2100, channel model, peer-to-peer.

I. Introduction

The channel model from COST 273 [1], and its successor COST 2100 [2], is now available and can account for most of the important propagation processes and effects that influence multiple-input multiple-output (MIMO) system performance. The COST 2100 channel model is characterized by individual clusters, i.e. group of multi-path components (MPCs), and corresponding visibility regions for the clusters [2]. The model supports both single-link and multiple-link MIMO channel access. The latter is achieved by using the concept of common clusters, where the MPCs from multiple links arise from the same physical scatterers. However, parameterization of this generic model from measurements is not complete yet and only a few environments have been studied. For example, in [3], the parameterization of indoor environments for the COST 2100 channel model has been performed though some parameters like cross-correlation coefficients between cluster spreads and cluster shadowing are missing. Similarly, only few studies have been carried out for validating the channel model. One reason for this is that there is no general methodology to evaluate the validity of channel models, and the validation processes also depend on available measurement data and the nature and usage of channel models. In [4], validation of the COST 2100 channel model from large scale properties such as delay spread, angular spread has been carried out for an indoor environment and a good accuracy of the channel model has been shown.

So far the studies for the COST 2100 channel model mostly focus on indoor environments, but are missing for outdoor scenarios. For a good generic model, different environments should be included and completely parameterized. In addition, validation should be performed to determine the accuracy and limitations of the channel model in those environments as well.

The main contributions of this paper are the following:

- Cluster parameters and cluster time variant properties are obtained for the 300 MHz measurements by using a joint clustering and tracking algorithm.
- Parameterization of the COST 2100 channel model for single-link outdoor MIMO communication at 300 MHz is conducted.
- Validation of the COST 2100 channel model is performed for the considered scenario by means of comparison between simulated and measured delay spread, spatial correlation, singular value distribution and antenna correlation.

The remainder of the paper is organized as follows: Sec. II describes the 300 MHz outdoor measurement campaign. Sec. III introduces the joint clustering and tracking algorithm for the cluster extraction from the measurements. The parameterization for the COST 2100 single-link MIMO channel model in an outdoor scenario is performed in Sec. IV. Sec. V validates the channel model with single-link parameters. Finally, the summary and conclusions in Sec. VI wrap up the paper.

M. Zhu and F. Tufvesson are with the Department of Electrical and Information Technology, Lund University, Lund, Sweden, e-mail: *firstname.lastname@eit.lth.se*.

G. Eriksson is with Swedish Defence Research Agency, Linköping, Sweden, e-mail: *guneri@foi.se*.

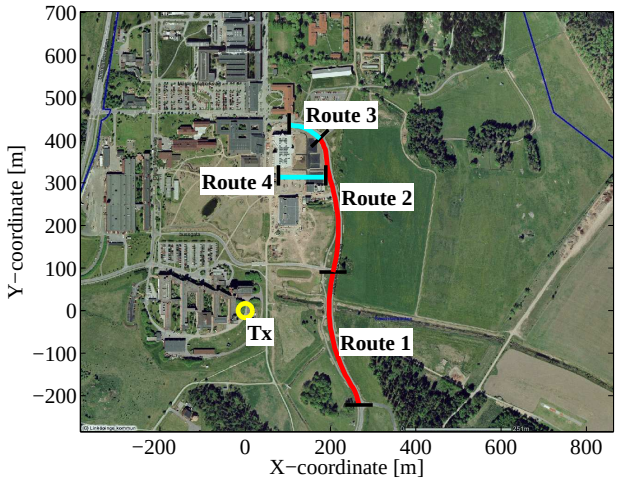

Fig. 1. Overview of the measurement area at the campus of Linköping University, Sweden. The transmitter with coordinate (0, 0) was placed near the building, and the receiver was moved along the marked routes.

II. Measurement Campaign

The measurements were performed outdoors on the campus of Linköping University, Sweden using the RUSK Lund MIMO channel sounder. An identical antenna array was used for both the transmitter and the receiver. The antenna array is a 7-element uniform circular dipole array (UCDA) with one additional dipole element located in the center at an elevated position. The transmit antenna (Tx) was placed 1.8 m above ground, at a static position with coordinate (0, 0) and about 35 m from a large building. The receive antenna (Rx) was mounted on a car and driven along four routes with lengths 322, 320, 80 and 110 m, see Fig. 1. The measurements were carried out at a center frequency of 285 MHz, and with a bandwidth of 20 MHz.

From the measured transfer function matrices, the properties (delay, angle of arrival (AOA), angle of departure (AOD), complex amplitude) of the MPCs were obtained by means of the SAGE algorithm [5]. From the analysis of [6], there were line-of-sight (LOS) conditions for route 1 and 2, which were in a more open area. Route 3 and 4, on the other hand, which were obstructed by buildings were completely non line-of-sight (NLOS). In the following analysis, routes 1 and 2 are processed together and named group 1, similarly route 3 and 4 are named group 2.

III. Clustering and Tracking Method

Since the COST 2100 channel model is based on the concept of clusters, a joint clustering and tracking algorithm [7] was used to identify the clusters and determine the cluster time properties from the measurements. The KpowerMeans clustering algorithm was used to cluster each temporal snapshot of the channel, while a Kalman filter [8] was used to track clusters from snapshot to snapshot. Previous research [9] has shown that the cluster time variant behaviors can be obtained with this joint algorithm.

MPCs extracted by the SAGE algorithm were used as the input to this joint clustering and tracking algorithm. First, the KpowerMeans clustering algorithm performs clustering based on the values of the delay, AOD, AOA and power of each MPC from one measured snapshot. The output of the clustering algorithm are clusters with the inter-cluster parameters (namely cluster centroid delay, AOD, and AOA, and cluster power), as well as the intra-cluster parameters (cluster delay spread, cluster AOD spread, and cluster AOA spread). The identified clusters for a particular snapshot are known as current clusters. In the next step, a Kalman filter was used to track the clusters over different snapshots. Based on the current clusters and clusters from the previous snapshot, the Kalman filter state was updated and the Kalman filter provided a prediction of cluster centriods for the next snapshot. Moreover, the current clusters were associated with the clusters from the previous snapshot and marked as tracked cluster if possible. Otherwise, untracked clusters in the previous snapshot are regarded as dead, and untracked clusters in the current snapshot were treated as new clusters. Hence we can obtain the cluster time variant properties such as the cluster lifetime, which is the time duration from the cluster's appearance until its disappearance.

In this paper, MIMO snapshots that were measured at fixed increments of 0.92 λ were taken into account when using the joint clustering and tracking analysis, where λ is the wavelength. The number of MPCs extracted with the SAGE algorithm is 200 for each snapshot; MPCs with a power 30 dB lower than the peak power were discarded for further analysis. To ensure tracking stability, a sliding window with length of 2 snapshots was chosen [7]. A 1% cluster power threshold was used to ensure that the identified clusters did not carry less than 1% of the total received power. In addition, if the power of a tracked cluster never exceeds 2.5% of the total received power during its lifetime, this tracked cluster was not accounted in the further analysis. In the clustering algorithm, the maximum cluster number was chosen as 12 to avoid cluster splitting; a large number of MPCs can be grouped into one large cluster but also distributed into several small clusters.

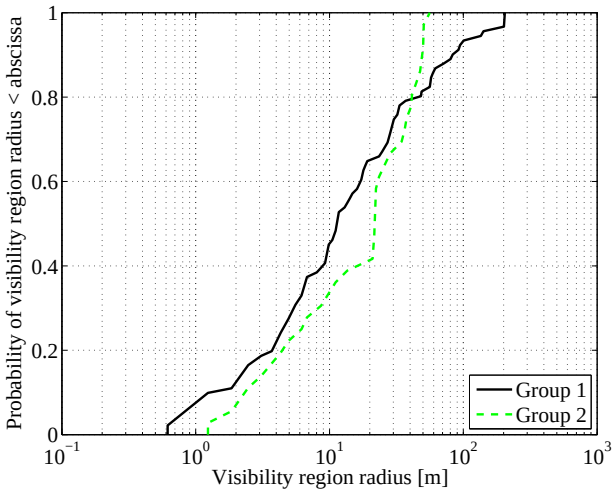

Fig. 2. Distributions of the extracted cluster visibility region radius for the two groups.

IV. Channel Model Parameters

In this section the parameterization methodologies for the COST 2100 channel model are studied in detail. Our goal is to extract the required parameters for the COST 2100 channel model based on the 300 MHz outdoor measurements and make the model work in the outdoor environments. All the extracted parameters are listed in Table I.

A. Cluster Visibility Region and Transition Region

Cluster visibility regions are typically assigned to clusters in such a way that when a Rx is inside a visibility region, the cluster assigned to this visibility region is active (contributes to the impulse response). The size of a visibility region is thus linked to the lifetime of a cluster: the lifetime of a cluster is determined by the number of snapshots over which the cluster is sequentially active.

There is a general difficulty in extracting the size of the visibility region from a single measured route. For the measured route, the Rx does not always go through the center of the visibility region. Assuming that the visibility region is a circle, and the radius of the circular visibility region R is deterministic. The product of the measured cluster lifetime and the snapshot distance is called cluster life distance L. If the radius of the visibility region is observed as half of the cluster life distance, a compensation factor should be considered. We propose the method for finding the compensation factor as follows. Assuming that the measured route "cuts through" the circular visibility region at a random (uniformly distributed) distance from the center of the visibility region; the relation between the measured average cluster life distance $E\{L\}$ and the extracted visibility region radius is obtained as

$$E\{L\} = \frac{\pi}{2}R. \tag{1}$$

We group the measurements into two categories. The measured scenario of group 1 is categorized as a semi rural environment and some scatterers have longer lifetimes, which lead to larger visibility region radii. The measured scenario of group 2, on the other hand, is categorized as a suburban area. In this group scatterers can be blocked more often and smaller visibility region radii are observed. Fig. 2 shows the distributions of the visibility region radii for the two groups. Most of the visibility region radii are in the range of 10 to 100 m (approximately 10 to 100 λ). The average visibility region radii for group 1 and 2 are 32.8 and 24.5 m, respectively.

There is a smooth transition when a cluster changes from active to non-active. The size of transition region is extracted from the cluster power attenuation versus the cluster lifetime. During the life of a cluster, when the power has decayed to 6 dB below the maximum power, then the cluster is seen to have entered the transition region, which lasts until the cluster is non-active. The radius of the transition region is obtained as half of the product of the snapshot distance and the number of transition snapshots. As for the discussion in the visibility region radius extraction above, a compensation factor in (1) should be taken into account as well. The average transition region radii for the two groups are 11.3 and 14.4 m, respectively.

B. Number of Clusters and Average MPCs per Cluster

There are two kinds of clusters in the COST 2100 channel model: local clusters and far clusters. Usually a local cluster occurs around the Rx. In our measurements, there is one active cluster which is visible during most of the snapshots for the two groups. At the same time, we notice that the distance between this cluster centroid and the Tx is larger than the distance

from the cluster centroid to the Rx. In addition, often there is a larger cluster angular spread at the Rx side compared to the Tx side. These observations indicate that we observe a Rx local cluster in the two measured groups. Far clusters are defined to be any clusters that are not local clusters. On average approximately 6 far clusters are active for both group 1 and 2.

Each cluster contains several MPCs, the average number of MPCs per cluster is extracted as the ratio between the total number of MPCs and the number of clusters in each snapshot. There are approximately 27 and 48 MPCs per cluster for group 1 and 2, respectively. For group 2, more scatterers exist and lead to a larger number of MPCs per cluster compared to group 1. Here it should be noted that specular components and dense multi-path components [10] are not separated, and all used MPCs are considered as specular components.

C. Single-bounce and Multiple-bounce Clusters

Besides local clusters and far clusters, "single-bounce" and "multiple-bounce" clusters are also distinguished in the COST 2100 channel model. Here we suggest one method to separate single- and multiple-bounce clusters by using the cluster geometric properties. First we take a look at the AOA and AOD of the cluster centroid and determine whether a ray from the Tx in the AOD direction and a ray from the Rx in the AOA direction can meet each other or not. If there is no valid intersection point between the two rays, a multiple-bounce cluster is observed. With a valid intersection point, we analyze the total traveling time of these two rays. The traveling time from the Tx to the cluster centroid is τ_{Tx} and from the Rx to the cluster centroid is τ_{Rx}. Theoretically, for a single-bounce cluster the difference between the total traveling time of the two rays and the cluster centroid delay τ_{delay} should be zero, but with the measured results, a threshold is set according to the environments. The threshold here is set as two times over the cluster delay spread τ_{ds}, since we allow one delay spread offset from both the Tx and the Rx side. In other words, if a valid intersection point between rays from the Tx and the Rx sides is obtained, and $|\tau_{\mathrm{Tx}} + \tau_{\mathrm{Rx}} - \tau_{\mathrm{delay}}| < 2\tau_{\mathrm{ds}}$ is satisfied, a single-bounce cluster is observed, otherwise it is certainly a multiple-bounce cluster. The relation of the number of single-bounce clusters N_{SB} and the number of multiple-bounce clusters N_{MB} is characterized by the cluster selection factor K_{sel},

$$K_{\mathrm{sel}} = \frac{N_{\mathrm{SB}}}{N_{\mathrm{MB}} + N_{\mathrm{SB}}}. \tag{2}$$

The estimated cluster selection factors are 0.1 and 0.2 for group 1 and 2, respectively. We conjecture that these low K_{sel} factors are due to the fact that the scenario is peer-to-peer, where the Tx and the Rx antennas are only around 2 m above ground, and both surrounded with scatterers along most of the measured routes.

The concept of cluster link delay is introduced in conjunction with the multiple-bounce clusters. The cluster link delay is calculated as $|\tau_{\mathrm{Tx}} + \tau_{\mathrm{Rx}} - \tau_{\mathrm{delay}}|$. Hence, for single-bounce clusters there is no cluster link delay. The link delay is modeled as an exponential distribution, with its mean and minimum cluster link delay [2]. Since we use $2\tau_{\mathrm{ds}}$ as our threshold when distinguishing single/multiple-bounce clusters, the cluster link delay for multiple-bounce clusters never goes below $2\tau_{\mathrm{ds}}$. The extracted average cluster link delays are 0.9 μs and 1.1 μs with minimum values 0.048 μs and 0.052 μs for group 1 and 2, respectively.

D. LOS Parameters

The LOS component is extracted based on AOA, AOD and the strongest received power among all MPCs. In theory, the AOA and AOD of the LOS component should match each other. However, due to uncertainties in vehicle positions and estimation errors of MPC parameters there might be an offset in the measured AOA and AOD. Here, maximum 10 degrees mismatch for the AOA and AOD is allowed. In other words, when the mismatch between AOA and AOD of the MPC with the strongest power is smaller than 10 degrees, we will treat this MPC as the LOS component.

The size of the LOS visibility region is extracted based on the appearance of the LOS component. When the power of the LOS component goes 6 dB below the maximum LOS power during its lifetime, it enters the transition region where it stays until it disappears. The transition region of the LOS component is defined as the duration between the transition starting and ending points. For group 1, the LOS component exists for almost the whole Rx traveling route; 343 m is observed as the LOS visibility region radius and 93 m as the LOS transition region radius. There is no LOS component in group 2, the size of LOS visibility and transition regions are set to zero.

The relation between power of LOS and other MPCs is denoted as LOS power factor [1],

$$K_{\mathrm{LOS}} = \frac{P_{\mathrm{LOS}}}{P_{\mathrm{tot}} - P_{\mathrm{LOS}}}, \tag{3}$$

where P_{LOS} is the power of the LOS component and P_{tot} is the total power for all MPCs. The observed mean K_{LOS} factor is -4.7 dB for group 1 and with variance 2.0 dB. In group 2, K_{LOS} is zero since it is a NLOS scenario.

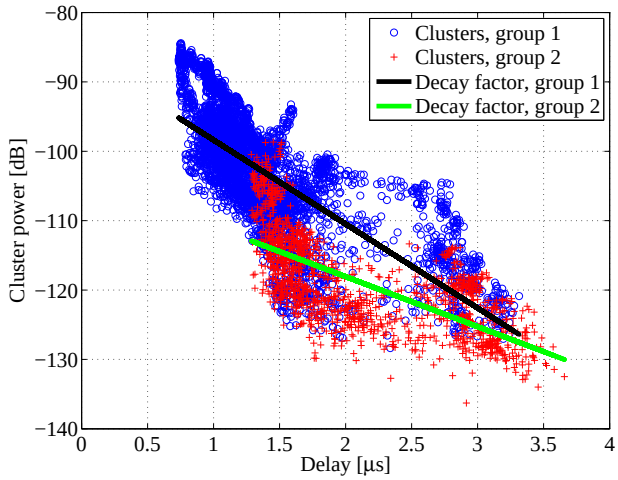

Fig. 3. Cluster power decay factor. Scatter plots show the cluster power vs. the cluster centriod delay. Two different power decay factors are observed.

E. Cluster Power Model

The cluster power of the mth cluster, P_m, is modeled as [1]

$$P_m = P_0 \max\{\exp(-k_\tau(\tau_m - \tau_0)), \exp(-k_\tau(\tau_\mathrm{B} - \tau_0))\}. \quad (4)$$

Besides the peak cluster power P_0 factor, there are three more parameters in this power model. Parameter k_τ is the power attenuation coefficient given in unit of $\mathrm{dB}/\mu s$, also called cluster power decay factor. The second parameter τ_0 is the delay of the LOS component with unit of μs and last one is the cut-off delay, τ_B, with unit of μs.

The cluster power decay factor is a result of linear regression analysis of the cluster power versus the cluster centroid delay. The slopes in Fig. 3 describe the power decay factors, which are 12.1 $\mathrm{dB}/\mu s$ and 7.2 $\mathrm{dB}/\mu s$ for group 1 and 2, respectively. The delay of LOS component is determined by the distance between the Tx and Rx. After exceeding the cut-off delay, the cluster power is modeled as constant. The cut-off delay is determined as the break point when a 30 dB power attenuation compared to the maximum cluster power is observed. From the measurements, cut-off delays of 2.4 μs and 4.2 μs are observed for group 1 and 2, respectively.

F. Cluster Spreads

The cluster spreads in delay, AOD and AOA are defined as [1]

$$DS_\mathrm{c} = \sqrt{\frac{\sum_i^{N_\mathrm{c}} P_i(\tau_i - \bar{\tau})^2}{\sum_i^{N_\mathrm{c}} P_i}}, \quad (5)$$

$$AS_\mathrm{c} = \sqrt{\frac{\sum_i^{N_\mathrm{c}} P_i(\varphi_i - \bar{\varphi})^2}{\sum_i^{N_\mathrm{c}} P_i}} \quad (6)$$

where DS_c is cluster delay spread, AS_c is cluster angular spread and N_c is number of MPCs in each cluster. Furthermore, P_i is the power for the ith MPC, $\bar{\varphi}$ and $\bar{\tau}$ are power weighted means calculated as

$$\bar{\tau} = \frac{1}{\sum_i^{N_\mathrm{c}} P_i} \sum_i^{N_\mathrm{c}} P_i \tau_i \quad (7)$$

$$\bar{\varphi} = \mathrm{angle}(\sum_i^{N_\mathrm{c}} P_i \exp(j \cdot \varphi_i)), \quad (8)$$

where j is the imaginary unit, τ_i is the delay and φ_i is the AOD/AOA of ith MPC. The cluster spreads for a particular cluster is computed from the set of MPCs that has been associated with that cluster. The mean value and standard deviation for the extracted spreads are listed in Table I. It can be noted that the average cluster delay and angular spreads are smaller in group 1 compared to group 2. The reason is that in group 2, we have rich scattering which increases the spread of the clusters. The MPCs from scatterers near the Rx in group 2 can for example have really large angular spread but are still grouped into one cluster.

TABLE I
EXTRACTED PARAMETERS FOR THE CHANNEL MODEL.

Groups	Group 1	Group 2
Radius of visibility region		
μ_{VR}[m]	32.8	24.5
Radius of transition region		
μ_{TR}[m]	11.3	14.4
Number of clusters		
μ_{Nc}	6	6
Number of MPCs per cluster		
μ_{MPCs}	27	48
Cluster selection factor		
$\mu_{\mathrm{K_{sel}}}$	0.1	0.2
Cluster power decay factor		
$\mu_{\mathrm{K_{decay}}}[\mathrm{dB}/\mu s]$	12.1	7.2
$\tau_{\mathrm{cutoff}}[\mu s]$	2.4	4.2
Radius of LOS visibility region		
μ_{VR}[m]	343	0
Radius of LOS transition region		
μ_{TR}[m]	93	0
LOS power factor		
$\mu_{\mathrm{K_{Los}}}$[dB]	-4.7	0
$\sigma_{\mathrm{K_{Los}}}$[dB]	2.0	0
Cluster angular spreads		
μ_{AOD}[deg]	14.6	18.6
σ_{AOD}[dB]	2.43	2.02
μ_{AOA}[deg]	14.8	19.0
σ_{AOA}[dB]	2.68	2.03
Cluster delay spread		
$\mu_{\mathrm{DS}}[\mu s]$	0.14	0.32
σ_{DS}[dB]	3.66	2.05
Cluster link delay		
$\tau_{\mu_{\mathrm{link}}}[\mu s]$	0.85	1.02
$\tau_{\mathrm{link,min}}[\mu s]$	0.048	0.052
Cluster shadowing factor		
σ_{Shf}[dB]	2.05	2.27
Cross-correlation coefficients		
$\rho(DS, AS_{\mathrm{AOD}})$	0.9	0.9
$\rho(DS, AS_{\mathrm{AOA}})$	0.9	0.9
$\rho(DS, Shf)$	0.0	-0.1
$\rho(AS_{\mathrm{AOD}}, Shf)$	0.0	0.1
$\rho(AS_{\mathrm{AOA}}, Shf)$	0.0	0.1
$\rho(AS_{\mathrm{AOD}}, AS_{\mathrm{AOA}})$	0.9	0.9

μ denotes expected value and σ denotes standard deviation.

G. Cluster Shadowing Factor

The clusters experience large-scale fading in a similar way as MPCs. The cluster shadowing factor is obtained during the process of estimating the cluster power decay factor, see Sec. IV-E. When the cluster power decay factor is estimated, the deviation for each cluster from the linear regression line can also be obtained, and defined as shadowing factor for clusters [11]. Note, however, that this "shadowing" is not necessarily related to the physical effect of partial obstruction of clusters by other objects. The observed standard deviations of shadowing are 2.05 dB and 2.27 dB for group 1 and 2, respectively.

H. Cross-correlation Coefficients

In order to jointly model cluster spreads and shadowing, the cross-correlation coefficients of different pairs of the cluster spreads and shadowing are considered. We estimate the cross-correlation coefficient between a and b as

$$\rho\langle a,b\rangle = \frac{\sum_i^N (a(i)-\bar{a})(b(i)-\bar{b})}{\sqrt{\sum_i^N (a(i)-\bar{a})^2 \sum_j^N (b(j)-\bar{b})^2}}, \tag{9}$$

where $\bar{a}$ and $\bar{b}$ are the sample mean of the set $\{a\{i\}\}$ and $\{b\{i\}\}$ with length N, respectively, and all the values are in logarithmic scale [12]. The results for the extracted cross-correlation coefficients are shown in Table I. A high correlation always exists between the delay spread and the angular spreads at both the Tx and Rx sides. Meanwhile, the cluster spreads exhibit small correlation with the cluster shadowing.

V. CHANNEL MODEL VALIDATION

The COST 2100 channel model with parameters according to Table I is validated by comparing the properties of its output with the corresponding measured channel for the outdoor single MIMO link at 300 MHz in this section. Ideally, one should

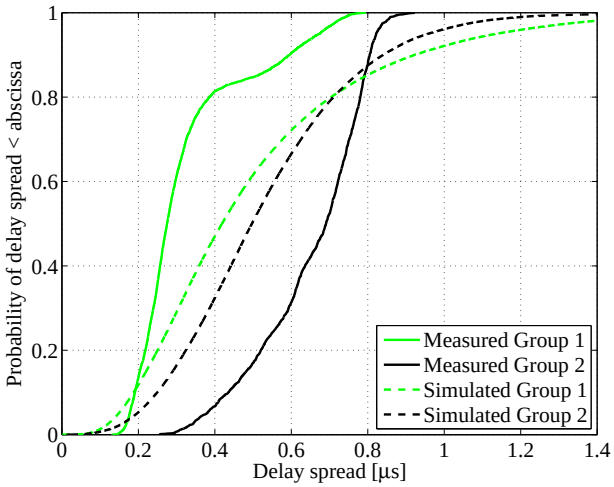

Fig. 4. Delay spreads of the measured and simulated omni-direction antenna responses for group 1 and 2.

perform validation based on many independent measurements in similar but different environments, but due to the efforts involved in such a task, this is not practically possible. The comparison with the measurements is performed for the following four channel properties: 1) delay spread, 2) spatial correlation, 3) singular value distribution, and 4) antenna correlation.

The COST 2100 channel model has been implemented in MATLAB by Liu *et al.* [13], and this implementation provides a nice framework for our validation. The input to this framework is based on both external and stochastic parameters. First the external parameters such as frequency, bandwidth, and so on are initialized as follows. The simulated area is defined as a cell with a radius of 500 m. Based on the cluster power decay factors derived in Sec. IV-E, we assume that clusters outside this radius will give a negligible contribution to the channel response. The Tx is placed in the cell center and the Rx is moving according to the measured routes. To be directly comparable with the measured data, the center frequency is set to 285 MHz and the channels are generated for a bandwidth of 20 MHz. In order to evaluated the detail of delay spread and spatial correlation, channel realizations are generated for every 0.12 λ movement of the Rx in the simulation. For each simulation run, this sampling distance gives us 5312 realizations with LOS condition (for the group 1 measurements), and 1560 realizations with NLOS condition (for the group 2 measurements). Besides the external parameters, Table I summaries all the stochastic parameters that are used as input of the MATLAB framework. An evaluation of 100 independent simulation runs is carried out, and we also verify that these 100 realizations are enough to get the statistical performance of the validated four properties.

A. Delay Spread

First we compare simulated and measured channels concerning their respective delay spreads. The comparison is performed for channel responses with an omni-directional antenna. In the measurements, the omni-directional antenna responses are from the central antenna elements of the Tx and Rx arrays. We compute the delay spread from the channel power delay profiles (PDPs) by using a noise threshold of 30 dB below the peak power in each PDP. In addition, all PDPs are truncated at 6 μs, where is can be assumed that no significant power will be received.

The results are shown in Fig. 4, where the dashed lines are cumulative distribution functions (CDFs) for the delay spreads from all independent simulation runs, and the solid lines, are CDFs for the delay spreads extracted from the measured raw data. Group 1, which has mostly LOS condition, has smaller delay spreads than group 2, which is under NLOS condition. The difference between LOS and NLOS is well reflected in the simulated channels. However, we find that the CDFs for the simulated channels start at smaller delay spreads than the corresponding CDFs for the measured channels. Furthermore, the distributions for the simulated channels have tails with significantly larger delay spreads than what can be observed from the two measured groups. But we have to keep in mind that the measurement is just a particular case and the COST 2100 model has the possibility to reproduce the same properties of the measurement. Here we are more interested in the statistical properties for the environment.

To understand the mechanisms behind the observed deviations between the simulated and measured delay spread distributions, we have investigated the shape of individual PDPs from simulations and measurements in some detail. First, in the upper plot of Fig. 5, we show an example of a case in which the PDPs of simulated and measured channels agree quite well. The PDPs indicate a channel with rather dense multi-path propagation. Next, in the lower plot of Fig. 5, two examples of PDPs from simulated channels with delay spreads that deviate significantly from what have been observed in the measurements are shown; one of the profiles leads to a very small delay spread and the other one causes a very large delay spread. The profile leading to the small spread has contributions from only the LOS component and the local cluster, no far clusters are present. Here we find a limitation of the COST 2100 channel model in the outdoor scenario. In reality in a built up area, as the measurements

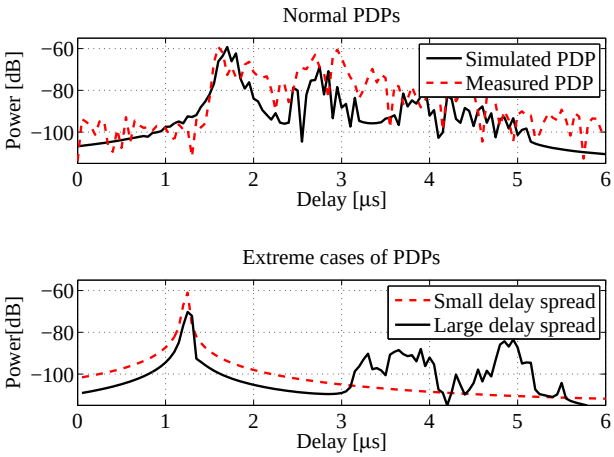

Fig. 5. PDPs. Upper: Simulated and measured PDP of a well represented channel. Lower: Simulated PDPs for channels with very small and large delay spread.

indicate, it is not likely to have only one cluster active in the outdoor scenario with a few objects somewhere around the Tx and/or Rx. In the large delay spread case, a large gap exists between the local cluster and the far clusters. This gap, which causes the delay spread to increase significantly, is observed in our simulation. In reality, however, the PDP for such a scenario is closer to a continuous decay without large gaps. In the channel model, the radius of a cluster is generated according to a log-normal distribution, and thus some small radii exist. As a consequence, the MPCs inside the clusters with small radii are compacted into a small delay region, which causes the gap in the PDP. In conclusion, we find that a truncated log-normal or log-uniform distribution provides a better fit for the distribution of delay spreads in an outdoor scenario.

B. Spatial Correlation

The channel responses are calculated based on the omni-directional antenna element for the two groups. The spatial correlation is evaluated for the channel envelope as follows:

$$R(\Delta d) = \frac{1}{N_d N_f} \sum_d \sum_f \frac{C(|H(d,f)|, |H(d+\Delta d, f)|)}{\sqrt{C(|H(d,f)|)C(|H(d+\Delta d,f)|)}}, \tag{10}$$

where f is the frequency, d is the relative distance of a certain snapshot to the first snapshot, Δd is the distance difference between two snapshots, C means the covariance and $|H|$ is the envelope of the channel. We choose the envelope correlation because that a oscillatory behavior of the averaged complex amplitude correlation is observed when the measured route is symmetric refer to the Tx, like route 1 and 2 in group 1, which is not representable. In this paper, we investigate the correlation properties for the distance differences from 0 to 10 wavelengths. The data is divide into small subsets with size of 12 wavelengths to keep the wide-sense stationarity (WSS) and a sliding window of 1.2 wavelength is used as well.

In Fig. 6, it can be noted that the difference between the simulation and measurement is not so significant, and we can say they have fairly good match. The simulation has high correlation within a quarter wavelength while the measurement shows high correlation within half wavelength. The spatial correlation is mostly determined by the distribution of the AOA spread of the MPCs. In general, a large angular spread leads to a low spatial correlation. In group 1, MPCs reach the Rx with small angular spread since the scatterers are located quite close to the direction of the LOS component; the averaged measured AOA spread is around 39 degrees. In group 2 more scatterers surround the Rx, and an AOA spread with 68 degrees is observed. Compared to group 1, this AOA spread is relatively larger and leads to lower spatial correlation. In the simulations, on the other hand, the cluster is placed uniformly in the cell; the AOA spread of all MPCs is not controlled, so the spatial correlation is reduced compared to the measurements. On the other hand, the size of cluster visibility region also affects the spatial correlation; longer visibility region radius gives higher similarity in different snapshots. In Sec. IV-A, some clusters have really long visibility region radii, e.g. the local cluster, though many clusters have short visibility region radii. The extracted average cluster visibility region radius cannot well reflect the real measurement environment, which leads to the mismatch in the spatial correlation as well. The variations of the visibility region radius cannot be accurately described only by an average value and a distribution function is suggested in outdoor environments for the COST 2100 channel model.

C. Singular Value Distribution

The channel model shows a good agreement with the measurements in terms of the distributions of the singular values obtained from the channel matrices, and thus of the channel capacity, see Fig. 7. For the singular value extraction, 7-by-7 channel transfer functions are generated for the two groups based on the model and measured antenna calibration data. All

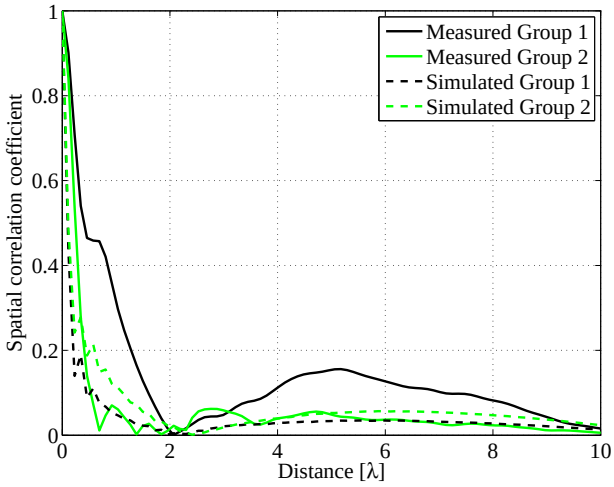

Fig. 6. Spatial correlation coefficient for the envelope of the channel.

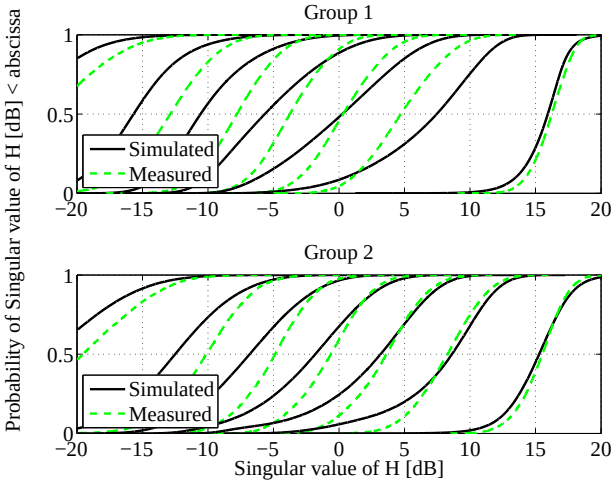

Fig. 7. Distributions of ordered singular values of the measured and simulated channel impulse responses.

singular values are evaluated with 20 dB SNR. Seven singular values are extracted for the 7-by-7 channel matrix. The dominant singular value and the second largest singular value match well with the measured data in each group. The fourth singular value is nearly 20 dB lower than the largest singular value in each group, and the contribution to the channel characteristics is insignificant. It can thus be noted that the COST 2100 channel model provides a good model of the measured channel regarding channel capacity.

D. Antenna Correlation

The correlation coefficients for different antenna element offsets are extracted from the measured and simulated channel frequency responses by clockwise and counter-clockwise shifting. A sliding window of length 20 λ is used to ensure that we remain in a WSS region when evaluating the antenna correlation. The averaged results over different WSS regions for all samples are shown in Fig. 8 and Fig. 9 for group 1 and 2, respectively. The upper plots of the two figures are the simulated absolute values of the complex antenna correlation coefficients and the lower ones are extracted from measurements. Here we only analyze one independent simulation over the outdoor geometrical area. Otherwise, in a long term, the antenna correlation will finally become low due to the uniform cluster distribution in the channel model.

In group 1, at the Tx side, good agreements between the simulation and measurement are achieved. However, some mismatch is obtained at the Rx side. In the measurement, group 1 has a LOS component and the AOA spread of MPCs is only 39 degrees, which lead to the high antenna correlation. But in the simulation, the clusters are placed uniformly in the cell which causes the large angular spread at the Rx side, and leads to the lower Rx antenna correlations. In group 2, the simulation shows a lower antenna correlation than the measurement at the Tx side though at the Rx side it shows a good match. It can be noted that the measured angular spread at the Tx side is quite small, while the AOD is more dominated by the trees and buildings in the upper north direction, see Fig. 1, and a higher antenna correlation is observed. However, for the simulation,

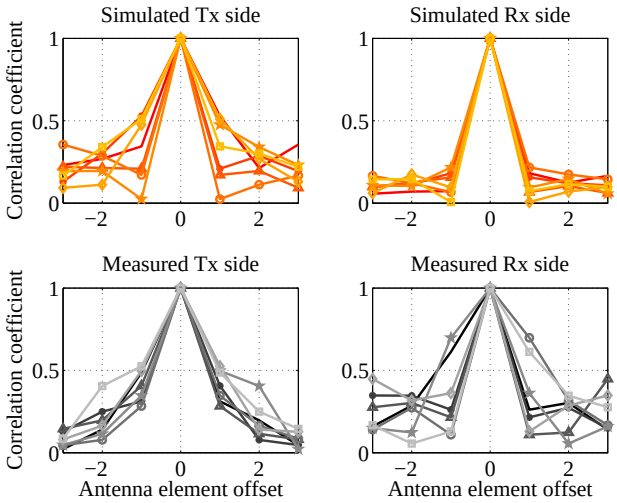

Fig. 8. Antenna correlations of the measured and simulated 7-by-7 MIMO channel for group 1.

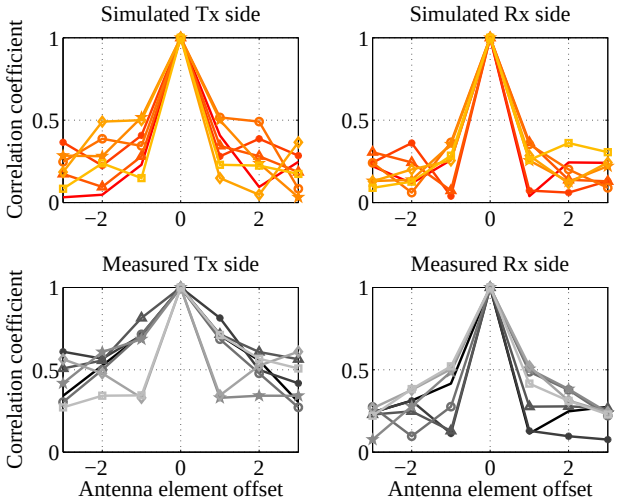

Fig. 9. Antenna correlations of the measured and simulated 7-by-7 MIMO channel for group 2.

the uniformly distributed clusters always have a large effect on the antenna correlation. In general, when the measured AOD or AOA are nearly uniformly distributed, a good matched antenna correlation from simulation can be obtained from the COST 2100 channel model.

VI. Conclusion

Table I summarizes the stochastic parameterization of the outdoor MIMO measurements at 300 MHz for the COST 2100 channel model. Parameterization of the size of visibility region is modified and additional parameterization of shadowing and correlation coefficients are discussed and analyzed in relation to the indoor parameterization. These parameters provide a basis for the COST 2100 channel model in outdoor environments. By using the parameters extracted from the 300 MHz MIMO measurements and the COST 2100 MATLAB channel model, we perform the validation by four means: delay spread, spatial correlation, singular value distribution and antenna correlation. The simulated and measured channels show a reasonable level of agreement, and the validation processes provide a deep insight of the COST 2100 channel model behavior for outdoor environments. In general, the COST 2100 channel model works well for representing the 300 MHz outdoor scenario, however, not all the properties show good agreements. We suggest that with the modifications and adjustments of the COST 2100 channel model, see Table II, better results can be obtained. The COST 2100 channel model also provides multi-link access, and studies related to multi-link will be carried out in the future.

VII. Acknowledgements

We thank Prof. Andreas F. Molisch for his helpful discussions and suggestions. The authors would also like to acknowledge Dr. Shurjeel Wyne for his clustering implementation and Dr. Ruiyuan Tian for his discussions of the cluster tracking algorithm.

TABLE II
MODIFICATIONS OF THE COST 2100 CHANNEL MODEL FOR THE 300 MHZ OUTDOOR SCENARIO.

Parameters	In the model	Adjustments
Cluster delay spread	log-normal	truncated log-normal/ log-uniform
Cluster visibility region	mean	mean and variance

REFERENCES

[1] L. M. Correia, "The COST 273 MIMO channel model," in *Mobile broadband multimedia networks*, Academic press, pp. 364-384, 2006.

[2] R. Verdone and A. Zanella, "Radio channel modeling for 4G networks," in *Pervasive mobile and ambient wireless communications: COST Action 2100 (signals and communication technology)*, Springer, pp. 67-148, 2012.

[3] J. Poutanen, K. Haneda, L. Liu, C. Oestges, F. Tufvesson, and P. Vainikainen, "Parameterization of the COST 2100 MIMO channel model in indoor scenarios," in *Proc. EuCAP 2011*, Rome, Italy, Apr. 2011.

[4] K. Haneda, J. Poutanen, L. Liu, C. Oestges, F. Tufvesson, and P. Vainikainen, "Comparison of delay and angular spreads between channel measurements and the COST 2100 channel model," in *Proc. LAPC 2010*, Loughborough, UK, Nov. 2010.

[5] B. H. Fleury, M. Tschudin, R. Heddergott, D. Dahlhaus, and K. Ingeman Pedersen, "Channel parameter estimation in mobile radio environments using the SAGE algorithm," *IEEE J. Select. Areas Commun.,* vol. 17, pp. 434-450, Mar. 1999.

[6] G. Eriksson, F. Tufvesson, and A. F. Molisch, "Propagation channel characteristics for peer-to-peer multiple antenna systems at 300 MHz," in *Proc. IEEE GLOBECOM 2006,* San Francisco, USA, Nov. 2006.

[7] N. Czink, R. Tian, S. Wyne, F. Tufvesson, J. Nuutinen, J. Ylitalo, E. Bonek, and A. F. Molisch, "Tracking time-variant cluster parameters in MIMO channel measurements," in *Proc. ChinaCom 2007*, Shanghai, China, 2007.

[8] S. M. Kay, "Kalman filters," in *Fundamentals of Statistical Signal Processing, Estimation Theory*, Prentice Hall, pp. 419-476, 1993.

[9] N. Czink, R. Tian, S. Wyne, G. Eriksson, T. Zemen, J. Ylitalo, F. Tufvesson, and A. F. Molisch, "Cluster parameters for time-variant MIMO channel models," in *Proc. EuCAP 2007*, Edinburgh, UK, Nov. 2007.

[10] J. Poutanen, J. Salmi, K. Haneda, V. Kolmonen, and P. Vainikainen, "Angular and shadowing characteristics of dense multipath components in indoor radio channels," *IEEE Trans. Antennas Propagat.,* pp. 245-253, Jan. 2011.

[11] S. Wyne, A. F. Molisch, G. Eriksson, P. Almers, J. Karedal, and F. Tufvesson, "Outdoor-to-indoor office MIMO measurements and analysis at 5.2 GHz," *IEEE Trans. Veh. Technol.*, vol 57, no. 3, pp. 1374-1386, May 2008.

[12] A. Algans, K. I. Pedersen, and P. E. Mogensen, "Experimental analysis of joint statistical properties of azimuth spread, delay spread, and shadow fading," *IEEE J. Select. Areas Commun.*, vol. 20, pp. 523-531, April 2002.

[13] L. Liu, N. Czink, and C. Oestges, "Implementing the COST273 MIMO channel model," in *NEWCOM-ACoRN Joint Workshop 2009*, Barcelona, Spain, Mar.-Apr. 2009.